

Automated Detection and Mitigation of Dependability Failures in Healthcare Scenarios through Digital Twins

Bruno Guindani*, Matteo Camilli*, Livia Lestingi*, Marcello M. Bersani*

*Dipartimento di Elettronica, Informazione e Bioingegneria
Politecnico di Milano, Via Ponzio 34/5, 20133 Milan, Italy

Email: {name}.{surname}@polimi.it

Abstract—Medical Cyber-Physical Systems (CPSs) integrating Patients, Devices, and healthcare personnel (Physicians) form safety-critical PDP triads whose dependability is challenged by system heterogeneity and uncertainty in human and physiological behavior. While existing clinical decision support systems support clinical practice, there remains a need for proactive, reliability-oriented methodologies capable of identifying and mitigating failure scenarios before patient safety is compromised. This paper presents M-GENGAR, a methodology based on a closed-loop Digital Twin (DT) paradigm for dependability assurance of medical CPSs. The approach combines Stochastic Hybrid Automata modeling, data-driven learning of patient dynamics, and Statistical Model Checking with an offline critical scenario detection phase that integrates model-space exploration and diversity analysis to systematically identify and classify scenarios violating expert-defined dependability requirements. M-GENGAR also supports the automated synthesis of mitigation strategies, enabling runtime feedback and control within the DT loop. We evaluate M-GENGAR on a representative use case study involving a pulmonary ventilator. Results show that, in 87.5% of the evaluated scenarios, strategies synthesized through formal game-theoretic analysis stabilize patient vital metrics at least as effectively as human decision-making, while maintaining relevant metrics 20% closer to nominal healthy values on average.

Index Terms—Human Digital Twin, Statistical Model Checking, Cyber-Physical Systems, Automata Learning

I. INTRODUCTION

Under hospitalized care, patients often interact with medical devices under the supervision of healthcare personnel. This patient-device-physician (PDP) triad constitutes a medical Cyber-Physical System (CPS) requiring strict operational safety and specialized design [23].

Medical practice defines the conditions under which a patient is considered clinically stable based on their vital parameters. We refer to situations in which the PDP triad cannot maintain such clinical stability as *failure scenarios*, whereas the PDP is said to be *dependable* when coordinated practitioner and device actions successfully preserve patient stability. Failure scenarios are commonly recognized and addressed by relying on human expertise and Clinical Decision Support Systems (CDSSs). CDSS software [53] supports clinicians by providing patient-specific knowledge and information to enhance care and reduce errors at multiple stages of the clinical process. Engineering automated monitoring and control mechanisms for such medical CPSs remains challenging due to the inherent complexity of their interacting components and the uncertainty of human decision-making,

which is influenced by individual expertise and environmental conditions. The US Institute of Medicine emphasizes that safe healthcare systems should “adopt a proactive approach that allows for examining processes of care for threats to safety” and incorporate mechanisms for “learning from errors” [45].

In this paper, we present an extension of GENGAR¹ [29], a methodology for the proactive identification of dependability failures in PDP CPSs. The approach adopts the Digital Shadow (DS) paradigm and combines automata-based modeling, data-driven learning of patient dynamics, and formal verification with model space exploration techniques to systematically uncover failure scenarios, where the PDP triad violates given *dependability requirements*.

Our extended version, referred to as M-GENGAR, complies with the Digital Twin (DT) paradigm [1]. As such, it enables a bidirectional digital representation of a physical system, where monitored data continuously updates the digital model, which can, in turn, influence the physical system through feedback and control. Beyond retrospective analysis, diagnostics, and monitoring, a DT enables simulation, prediction, and decision support by closing the loop between physical and digital domains. In addition to the identification of failure scenarios, our extension M-GENGAR supports: *i*) diversity analysis of failures by isolating distinct critical contingencies; *ii*) automated synthesis of response strategies to such critical contingencies; *iii*) alignment of the PDP model with data from the physical system (*feedback* action of the DT paradigm) upon failure detection; and *iv*) clinical decision support through the recommendation of optimal mitigation actions for ongoing failures (*control* action of the DT paradigm).

The PDP model at the core of our methodology captures the functions of medical equipment (including monitors for critical clinical metrics), the practitioner’s actions, the patient’s behavior, and all relevant interactions between the three entities by adopting Stochastic Hybrid Automata (SHA) [20]. Specifically, we use *hybrid* features to capture non-trivial dynamics of physiological quantities and *stochastic* features to approximate the sources of uncertainty due to human behavior (e.g., alternative practitioner decisions and delays or sudden changes in patient health). The SHA model is developed by relying on expert knowledge and field-collected data. For aspects subject to uncertainty (e.g., sudden changes in patient health), M-GENGAR uses the data-driven automata learning

¹Guided Exploration of iNterfaces and Guidelines Adhering to Requirements.

technique L_{SHA}^* [37], [38] to infer the patient model from real physiological logs.

The resulting parametric model represents a family of PDP triads and identifies a design space. A point in the design space (i.e., a value-assignment to the triad parameters) corresponds to a specific clinical scenario (e.g., the onset of an asthma attack). Our methodology explores the design space through fuzzing [41]. Starting from a reference model based on domain knowledge, multiple variants (mutants) are automatically generated to detect violations of dependability requirements (defined by domain experts). Specifically, each generated SHA mutant is analyzed through Statistical Model Checking (SMC) to calculate the probability that a requirement holds [36]. After filtering out unrealistic or clinically irrelevant scenarios, we analyze the diversity of the failures to isolate distinct root causes. SHA scenarios are converted to 1½-player-games to synthesize near-optimal strategies through UPPAAL STRATEGO [19], informing physicians on what actions to take to maximize the likelihood of satisfying the requirements.

We empirically evaluate the proposed methodology on a representative PDP exemplar involving a *patient* affected by lung disease, a pulmonary ventilator (the *device*), and an intensivist (the *physician*). Domain knowledge elicited through expert interviews informs both the physician–device model and the specification of dependability requirements, while patient data are generated using a high-fidelity physiological simulator [13]. The experimental campaign includes 10 hours of cumulative acquisition time, including both interviews and simulation sessions. Results show that, in 87.5% of the evaluated scenarios, the simulated physician guided by the synthesized strategies stabilizes patient vital metrics at least as effectively as the human physician, while maintaining the relevant metrics 20% closer to their nominal healthy values.

In summary, compared to our prior work [29], the main contributions are:

- an online clinical decision support phase upgrading the previous DS to a fully fledged DT infrastructure with real-time state alignment and action selection;
- a diversity analysis of failure scenarios to isolate different root causes;
- an automated synthesis of control strategies that support medical personnel in selecting actions that ensure the dependability of the PDP system; and
- an extended empirical evaluation covering the newly added elements of the methodology.

The paper is structured as follows: Section II reviews preliminary concepts; Section III introduces the PDP exemplar serving as running example; Section IV details the developed methodology; Section V presents experimental results; Section VI discusses findings; Section VII surveys related work; and Section VIII concludes.

II. PRELIMINARIES

A. Formal Analysis

1) *Stochastic Hybrid Automata*: Hybrid Automata (HA) extend finite-state automata by including real-valued variables

that evolve continuously over time according to flow conditions specified by Ordinary Differential Equations (ODEs) [2], thus modeling systems with complex, non-linear dynamics. An HA is a tuple $\mathcal{H} = (\Sigma, L, X, F, E, I, P)$ where: *i*) Σ is a set of actions, partitioned into inputs (Σ_i) and outputs (Σ_o); *ii*) L is a set of locations, each representing a distinct operational mode of an agent or a physical phenomenon; *iii*) X is a set of real-valued variables governing system dynamics, and $G(X)$ is the set of constraints on X (e.g., $x < 10$); *iv*) $F = f_\ell : \ell \in L$ defines flow conditions, with each f_ℓ describing the time evolution of variables in X at location ℓ through a system of ODEs $\dot{X} = f_\ell(X)$; *v*) $E \subseteq L \times G(X) \times \Sigma \times 2^X \times L$ is a finite set of edges between locations, each including a guard from $G(X)$, an event from Σ , and an assignment to variables of X called *resets* (e.g., $x = 0$); *vi*) $I : L \rightarrow G(X)$ assigns *invariants*, i.e., constraints on X , to locations; *vii*) $P : L \rightarrow \mathbb{R}^+$ assigns exit rates to locations. Stochastic Hybrid Automata (SHA) extend HA with stochastic elements [20] that represent uncertainties in physical phenomena. For example, if parameter θ in a flow condition is treated as a random variable s.t. $\dot{X} = f(X, \theta)$ with $\theta \sim \mathcal{D}$, then X follows a stochastic process.

An SHA network consists of multiple SHAs that synchronize on actions in Σ , ensuring that all the involved automata take an edge simultaneously when an event occurs. Specifically, an SHA can trigger synchronization via an edge labeled $\sigma \in \Sigma_o$, while others react with $\sigma \in \Sigma_i$ at the same time.

2) L_{SHA}^* for SHA learning: Automata learning algorithms largely adopt the teacher-learner structure from L^* [3]. Our approach uses L_{SHA}^* , extending L^* to SHA [37], [38], where the training dataset consists of *signals*, i.e., sequences of timestamp-value pairs $(t_0, s_0), (t_1, s_1), \dots$, with $t_i, s_i \in \mathbb{R}$ and $0 \leq t_i \leq t_{i+1}$ for adjacent pairs.

Besides the training dataset, L_{SHA}^* requires: *i*) a set X_F of real-valued variables whose time dynamics are inferred and constrained by flow conditions; *ii*) a set Σ of actions corresponding to real-world events, whose relationship with changes in the dynamics of variables in X_F is learned from data; *iii*) a set X_M of real-valued variables used to extract events from the collected data. Each variable in X_F and X_M is associated with a signal in the dataset. A user-defined *labeling* partial function \mathcal{L}_{X_M} maps signals to traces (i.e., sequences of actions). Specifically, $\mathcal{L}_{X_M}(t) = \sigma \in \Sigma$ indicates the action corresponding to the event at timestamp t . L_{SHA}^* learns: locations L , edges E , flow conditions F for variables in X_F , and distributions \mathcal{D} for random parameters in the ODEs. The resulting SHA is suitable for formal verification and can serve as a predictor for variables in X_F , given the actions in Σ .

3) *Strategy Synthesis*: Strategy synthesis for SHA networks aims to derive an optimal *controller* policy that resolves nondeterminism to satisfy a quantitative reachability objective under stochastic uncertainty.

An SHA network is interpreted as a 1½-player timed game [18]. In contrast to classical 2-player games, the environment is stochastic rather than adversarial, and reachability objectives are therefore addressed via stochastic strategies over controllable actions. Accordingly, the output action alphabet is partitioned as *controllable* and *uncontrollable* $\Sigma_o = \Sigma_{o,c} \cup \Sigma_{o,u}$. A *stochastic strategy* is a density function

$\pi : L \times \mathbb{R}_+^X \times \mathbb{R}_+ \times \Sigma_{o,c} \rightarrow \mathbb{R}_+$, defining the likelihood of selecting a specific controllable action $\sigma \in \Sigma_{o,c}$ after a delay $d \in \mathbb{R}_+$ for any possible system configuration $(l, \nu) \in L \times \mathbb{R}_+^X$. Strategy synthesis reduces to a *cost-bounded reachability problem* that, given a bound $b \in \mathbb{R}_+^X$, entails the computation of a *stochastic strategy* guaranteeing the network reaches a *safe state*, i.e., a location in $G \subseteq L$ such that the accumulated costs are bounded by b . When dealing with stochastic strategies in timed games, it is common practice to restrict the scope to so-called *non-lazy strategies* [18], [21]. Informally, these strategies are designed to avoid “procrastination”, as they ensure that controllable discrete actions are not unnecessarily delayed when they contribute to reaching the goal. Instead of waiting for an arbitrary amount of time, a non-lazy strategy decides whether to act immediately or to wait for an environmental action, at any time instant. Non-lazy strategies can be effectively recast as deterministic strategies. For each configuration (l, ν) , one can simply select the most promising action. The deterministic choice maximizes the probability of success, effectively collapsing the stochastic distribution into a single, optimal decision. More formally, the resulting strategy derived from π is a mapping $\Pi : L \times \mathbb{R}_+^X \rightarrow \Sigma_{o,c}$. UPPAAL STRATEGO [19] is adopted in this work to model the reachability game and compute the stochastic strategy.

B. Fuzzing

Fuzzing [41] is an automated testing approach that systematically generates inputs. Instead of relying on manually crafted test cases, fuzzing explores a wide range of program behaviors to uncover defects, often using runtime feedback (e.g., code coverage) to guide the process. Inputs can be generated from scratch or derived from existing examples to reveal unexpected behavior, such as assertion violations.

Mutational fuzzing [11] produces new test cases by applying transformations to a set of valid inputs (seeds). This approach assumes that small modifications to valid inputs can trigger new behaviors while largely preserving validity. Feedback mechanisms, such as code coverage or estimated likelihood of failure, are used to prioritize mutations, enabling the fuzzer to incrementally explore untested behavior.

Search-based fuzzing (or testing) [10] extends mutational fuzzing by applying optimization strategies to guide input generation toward specific objectives. In this setting, test case generation is treated as an optimization problem, where candidate inputs are evaluated with a fitness function often based on execution depth, branch coverage, or proximity to requirements violations. Techniques like evolutionary strategies or genetic algorithms [22] allow the fuzzer to focus on input regions with higher potential to reveal failures.

III. RUNNING EXAMPLE: RESPIRATORY INTENSIVE CARE

Our scenarios of interest occur in the hospital Intensive Care Unit (ICU) and involve a patient with lung disease admitted to the ICU, the medical staff responsible for their care, and the mechanical ventilator (the device) operated by the staff to provide life support (see Fig. 1).

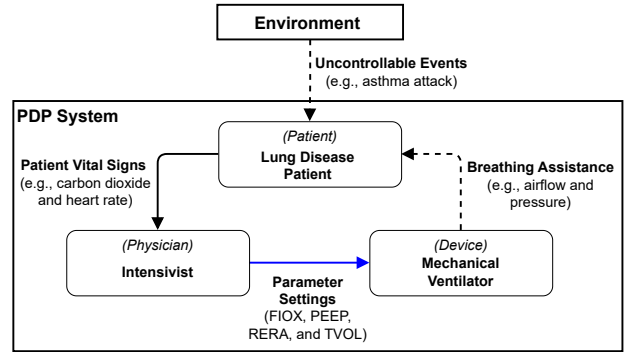


Fig. 1: PDP triad used as a running example showing interactions between the agents and the environment: an arrow from agent a to b represents an event that a triggers directed to b . Controllable events are in blue, uncontrollable but observable events are in solid black, while uncontrollable and not directly observable events are represented by dashed arrows.

TABLE I: Ventilator parameters.

acronym	full name	range	unit
FIOX	fraction of inspired oxygen	[0, 1]	N/A
PEEP	positive end-expiratory pressure	[5, 25]	cmH ₂ O
RERA	forced respiration rate	[6, 18]	min ⁻¹
TVOL	forced tidal volume	[300, 500]	mL

The intensivist can affect the patient’s respiratory state [46] by toggling the ventilator’s operation and adjusting the four parameters² in Table I [9]. Actions are applied to patients according to standard procedures [46], manipulating ventilator parameters to mitigate adverse events. Appropriate interventions are determined by the intensivist through continuous monitoring of patient’s key vital signs—carbon dioxide CD, heart rate HR, oxygen saturation OS, respiration rate RR, and tidal volume TV— with actions based on changes that require medical attention. As illustrated in Fig. 1, the intensivist has full control over the ventilator but cannot directly observe events affecting the patient’s health, inferring conditions such as an asthma attack through observed variations in vital signs.

This PDP triad forms a complex CPS, where human agents interact with cyber-physical devices and exercise judgment in operating them. Uncertainty arises from both human behavior (the physician’s decisions) and environmental events that influence the patient’s vitals (e.g., asthma attacks). These factors highlight the importance of DT paradigms capable of accurately modeling all agents in the PDP triad. Moreover, detecting and analyzing critical scenarios that reflect reductions in practitioner effectiveness through the DT can aid medical staff in preventing patient-threatening situations.

IV. METHODOLOGY

M-GENGAR identifies potentially critical scenarios that may endanger the patient’s health status (the *failures*), and synthesizes action strategies to provide the physician with

²TVOL values depend on patient characteristics such as body mass [46]. The reported range corresponds to values used in our experiments.

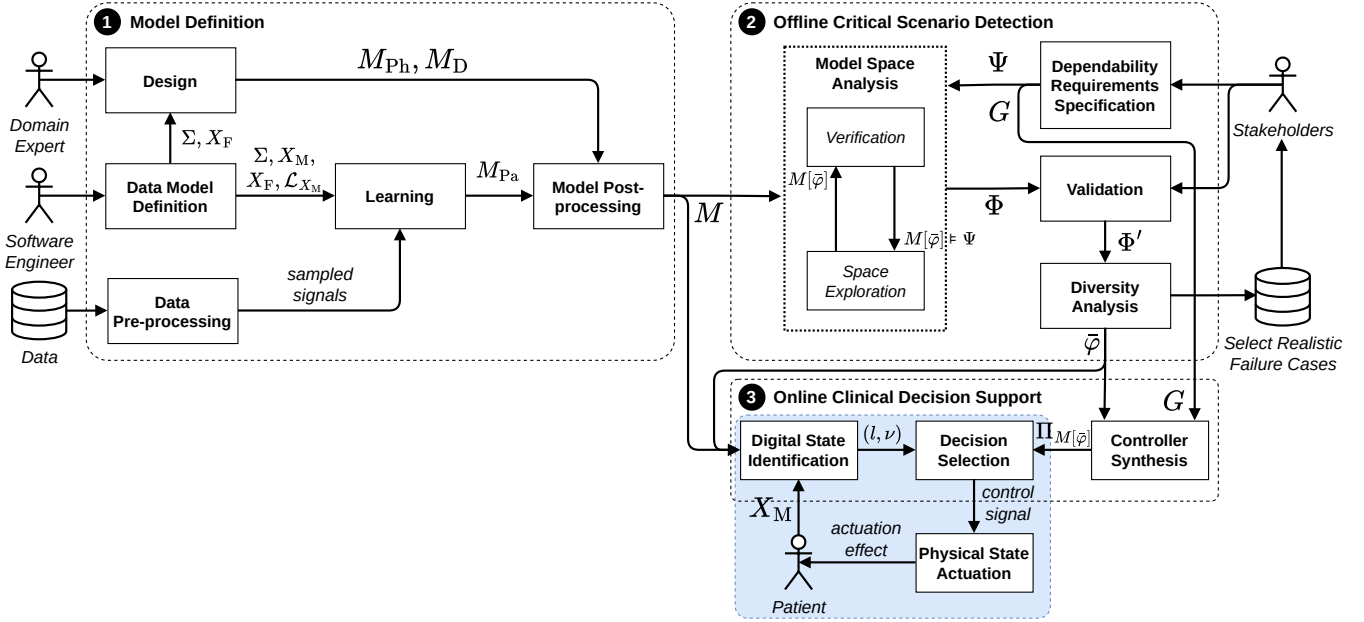


Fig. 2: Overview of proposed methodology, highlighting the three *phases* (dashed boxes), the data flow between phase *activities* (solid boxes), and the actors involved in activities requiring human input. The DT alignment loop is in blue.

clinical decision support. As depicted in Fig. 2, the methodology includes three phases and requires the collaboration of actors with a medical background (i.e., the *domain experts*) and technical expertise (i.e., *software engineers*). In particular, it generates models of PDP triads by leveraging domain knowledge and data collected in real-world settings (the **Model Definition** phase). Model are then analyzed to determine whether they satisfy set dependability requirements (the **Offline Critical Scenario Detection** phase). The resulting set of identified failures is filtered to remove redundancy and communicated to the *stakeholders* of the PDP system; these comprise professionals involved in both the clinical and organizational dimensions of care delivery, including clinicians and department directors, as well as individuals responsible for training medical staff or overseeing their performance [25].

Leveraging the generated models, our methodology synthesizes action strategies to support physician decision-making in the scenarios under scrutiny. These strategies can be integrated into a CDSS, constituting the **Online Clinical Decision Support** phase of the methodology, although no CDSS is deployed in this work. In a real-world setting, such a system would interface with the physical world by acquiring patient data, aligning the DT's state with the physical one, and actuating or suggesting clinical actions.

A. Model Definition

This phase produces an SHA representation of the PDP triad via a manual Design activity and an automated Learning activity. The Data Model Definition and Data Pre-processing activities must be carried out beforehand to provide well-formed inputs to the learning process. Finally, Model Post-processing refines the generated models to ensure their compatibility with the verification procedures employed in the subsequent phase.

1) *Data Model Definition*: As we make use of SHA (see Section II-A), the input required for the learning process includes the set of events Σ and the sets of physical quantities to be modeled. The selection is guided by domain expertise and informed by the operational capabilities and constraints of the available medical equipment, ensuring the learned model captures clinically meaningful and observable behaviors.

Among the selected variables, those that are continuously monitored and require accurate estimation (X_F) are modeled by flow conditions (F). Other variables (X_M) are primarily informative when they signal specific conditions of the patient or the surrounding environment, such as the violation of critical thresholds that typically trigger alarms on medical equipment, and are thus used for event identification. The labeling function \mathcal{L}_{X_M} maps scenario-dependent conditions on variables in X_M to events in Σ , thereby formally defining how real-world events are detected from data. Domain knowledge is essential here for identifying clinically relevant events through possibly complex activation criteria defined over the variables.

Example IV.1. Consider our running example in Section III. Events represent either a significant variation in the patient's vital signs or a change in ventilator settings performed by the intensivist. Accordingly, these quantities populate the set $X_M = V \cup P$, where $V = \{CD, HR, OS, RR, TV\}$ contains the patient's vitals and $P = \{FIOX, PEEP, RERA, TVOL\}$ includes the ventilator parameters. Each patient vital $v_i, i = 1, \dots, 5$, is associated with a safe operating range $R_i = [v_i^{\min}, v_i^{\max}]$. An event is observed when the value of vital i at time t_k (denoted as $v_i^{t_k}$) exceeds its safe range, indicating a deviation from normal physiological conditions, or when it returns within such range, signaling a possible recovery or stabilization. The ventilator parameters p_j , with $j = 1, \dots, 4$ (see Table I), trigger events whenever they are manually

increased or decreased by the intensivist. Finally, the events on and off correspond to the activation and deactivation of the mechanical ventilation device, respectively. When the device is inactive, all ventilator parameters are assumed to be set to zero. We define the partial labeling function \mathcal{L}_{X_M} as follows:

$$\mathcal{L}_{X_M}(t_k) = \begin{cases} (V_i)^{\text{high}} & \text{if } v_i^{t_k} > v_i^{\text{max}} \wedge v_i^{t_{k-1}} \leq v_i^{\text{max}} \\ (V_i)^{\text{low}} & \text{if } v_i^{t_k} < v_i^{\text{min}} \wedge v_i^{t_{k-1}} \geq v_i^{\text{min}} \\ (V_i)^{\text{ok}} & \text{if } v_i^{t_k} \in R_i \wedge v_i^{t_{k-1}} \notin R_i \\ (P_j)^{\text{up}} & \text{if } p_j^{t_k} > p_j^{t_{k-1}} \wedge p_j^{t_k}, p_j^{t_{k-1}} \neq 0 \\ (P_j)^{\text{down}} & \text{if } p_j^{t_k} < p_j^{t_{k-1}} \wedge p_j^{t_k}, p_j^{t_{k-1}} \neq 0 \\ \text{on} & \text{if } p_j^{t_k} > 0 \wedge p_j^{t_{k-1}} = 0 \forall j \\ \text{off} & \text{if } p_j^{t_k} = 0 \wedge p_j^{t_{k-1}} > 0 \forall j \end{cases}$$

for $V_i \in V, P_j \in P, k = 1, 2, \dots$

We select $X_F = \{\text{TV}\}$ as the variable modeled through flow conditions, since even minor variations in its value are critical for assessing the patient's ability to breathe.

2) *Data Pre-processing*: Raw input data are generally unsuitable for learning algorithms, as meaningful information is not immediately available and must therefore be extracted with proper processing. Smoothing noisy signals, resampling data to enforce uniform time intervals, or extracting salient features, such as peak values or rates of change, is customary to capture underlying physiological dynamics better.

Example IV.2. In our running example, we apply a smoothing transformation to the CD (carbon dioxide) signal, which naturally exhibits a sinusoidal breathing-induced pattern. The raw signal is transformed into a time series that records, at each time step, the most recent peak value observed. This peak-based representation attenuates high-frequency oscillations while preserving clinically relevant trends, yielding a signal that is more robust to noise and better aligned with the threshold-based event definitions used by the learning activity.

3) *Design*: Through structured interactions with domain experts (e.g., interviews), engineers elicit specifications of the interventions the physicians perform, the triggering events, and the contextual conditions required for each action. The collected knowledge allows them to formalize components of the PDP system by encoding established clinical practices for managing a patient's evolving health conditions, effectively capturing medical expertise. Their activity results in models for both the physician (M_{Ph}) and the ventilation device (M_D).

These elements are specified as a SHA, where interventions are modeled as actions on edges and care activities are represented as locations within the physician and device models. Guards on edges encode the contextual conditions required for executing each action. When multiple interventions are clinically admissible while the physician is treating the patient, M_{Ph} incorporates probabilistic edges with predefined weights, allowing the physician-device interaction model to capture the inherent variability of clinical decision-making.

The resulting SHA models are parameterized to represent the degrees of freedom in the intensivist's decision-making process. Model parameters, defined jointly by engineers and

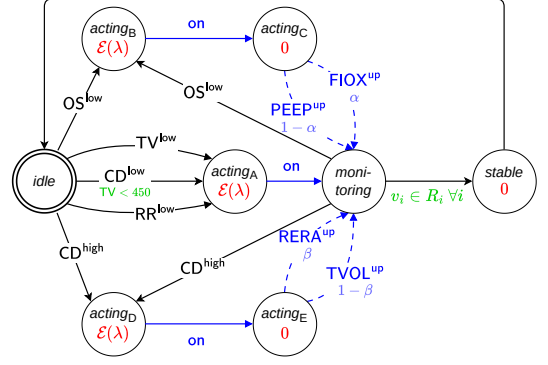


Fig. 3: Example of physician-device SHA.

the domain experts, govern key behavioral aspects of the triad and explicitly encode elements of human judgment and uncertainty. Different parameter instantiations may yield adverse or unsafe patient behaviors, making these parameters central to the Offline Critical Scenario Detection phase.

Example IV.3. Figure 3 shows a SHA obtained through expert elicitation. It models the behavior of an intensivist who reacts to clinical events (depicted with black labels on arrows) by activating the mechanical ventilator and adjusting its operational parameters. Physician-controlled edges are depicted with blue arrows and labels, while stochastic choices are represented by dashed edges annotated with probability weights. Guards are highlighted in green, and the distributions governing leaving times from locations are shown in red.

According to the model, the physician activates the ventilator (action on) when a decrease is detected in any of the vital signs TV, CD, or RR, provided the ventilator is inactive. In response to low oxygen saturation (OS) or elevated carbon dioxide (CD), the physician activates the ventilator and adjusts one of its parameters. For low OS, the physician probabilistically increases either FIOX or PEEP, with weights $(\alpha, 1 - \alpha)$; for high CD, the choice is between increasing RERA or TVOL, with probabilities $(\beta, 1 - \beta)$. The edge labeled CD^{low} has a guard $TV < 450$, ensuring the physician responds to a CD^{low} alarm only when tidal volume is below 450 mL. Once all vitals v_i return to their safe ranges R_i , the patient is considered stabilized, prompting a transition to the *stable* state, after which the physician returns to the *idle* state.

The SHA models realistic response delays for the physician using an exponentially distributed random variable with rate λ , while other actions are executed instantaneously. Observation states such as *idle* and *monitoring* lack physician-controlled outgoing transitions; exits from these states occur solely through patient-generated events, so no delay distribution is assigned. Model parameters are collectively denoted $\varphi = (\alpha, \beta, \lambda)$, where $\alpha \in [0, 1]$, $\beta \in [0, 1]$, and $\lambda \in [1/15, 1]^3$.

4) *Learning*: A data-driven model of patient behavior is essential to captures the evolution of physiological conditions over time and under clinical interventions. The patient model

³ α and β are probabilities, while the range for λ reflects realistic average ICU response times (in seconds), as informed by domain expertise.

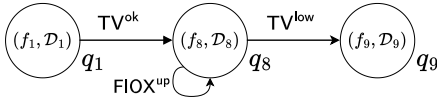


Fig. 4: Detail of learned patient SHA having 11 locations.

M_{Pa} complements the physician and device models, thereby completing the PDP triad.

Patient health conditions in ICUs are inherently complex and only partially observable, especially in the case of respiratory diseases whose underlying physiological mechanisms cannot be measured directly. Intensivists therefore rely on indirect indicators, such as vital signs acquired through monitoring equipment, to assess patient status and guide interventions. This partial observability, combined with inter-patient variability and stochastic physiological responses, motivates the learning of patient dynamics from empirical observations.

The Learning activity builds upon the artifacts defined during the data model definition phase, including the set of events, the physical variables, and the labeling function. It integrates raw physiological signals collected in the ICU, which may originate from medical devices, hospital information systems, or manual entries by healthcare professionals. To infer the patient model, M-GENGAR employs the automata learning algorithm L_{SHA}^* , which derives an SHA-based representation from clinical data. The algorithm infers both the discrete structure of the model (locations and edges) and the continuous dynamics associated with each location. Specifically, each learned location is equipped with a flow condition governing the evolution of the physical variables in X_F , together with a parametric probability distribution capturing stochastic variability. Locations thus correspond to distinct physiological states inferred from data, while edges represent clinically relevant events that drive changes between such states.

Example IV.4. Figure 4 illustrates a portion of the patient SHA model learned using L_{SHA}^* . The flow condition f_i and stochastic parameter distribution \mathcal{D}_i jointly govern the evolution of variable $TV \in X_F$ while the system resides in location q_i . From location q_1 , the occurrence of the TV^{ok} event, indicating that tidal volume has returned to safe levels, moves the patient to location q_8 . From there, event TV^{low} transitions the patient to location q_9 . The $FIOX^{up}$ self-loop represents that the physician’s action of increasing FIOX has no observable effect on the patient’s state while in q_8 .

5) *Post-processing*: The final activity of model definition combines the individual models of the PDP components (namely physician M_{Ph} , device M_D , and patient M_{Pa}) into a single, unified model representing the triad. This composite model is further refined to ensure compatibility with the verification procedures of the subsequent phase. The refinement produces the final model M as output.

Example IV.5. The patient model M_{Pa} learned from data is inherently incomplete, as not all locations necessarily contain outgoing edges for every event in Σ . While manually designed models can explicitly handle all possible events in every location, learned models typically reflect only the behaviors

observed during training. Some events may be left untreated in some locations if they never occurred during data collection.

Under such circumstances, typical post-processing includes ensuring the model is well-defined for all events, by introducing a *sink* location representing unmodeled or unsupported behaviors for which data is insufficient. For each location in M_{Pa} lacking an outgoing edge for some event $e \in \Sigma$, an edge labeled with e is added and linked to the sink location.

B. Offline Critical Scenario Detection

This phase evaluates whether the SHA digital model M satisfies the dependability requirements required by stakeholders. The Model space analysis activity leverages an initial specification of formal requirements to systematically explore variations of model parameter and structure. Candidate generation combined with formal verification enable the identification of failure-inducing configurations. Clinically unrealistic scenarios are filtered with the Validation activity, and through the Diversity analysis activity representative and meaningful critical scenarios are selected.

1) *Dependability Requirements Specification*: To identify and formalize the system properties guaranteeing patient safety and reliable treatment, engineers directly collaborate with stakeholders. The latter may include clinicians, who define relevant medical conditions; biomedical engineers, who specify equipment constraints; safety analysts, who ensure compliance with risk mitigation standards; and department directors, who focus on operational efficiency. This elicitation process allows domain experts to contribute expectations and operational constraints, which are then translated into verifiable properties. The specification language must support properties with a probabilistic interpretation over SHA models, enabling reasoning about uncertainty and temporal behavior in PDP triads.

The activity yields a set Ψ of dependability properties, each of which can be evaluated on a given SHA instance as satisfied or violated with an associated probability. Such probabilistic semantics enables the identification of scenarios in which dependability degrades under uncertainty. The activity also defines a reachability goal G , specified as a set of safe automaton states and a cost metric to minimize. Reachability of these states constitutes a dependability objective that will be exploited in the online clinical decision support phase.

Example IV.6. Consider again our running example presented in Section III. We define three dependability properties evaluated over a fixed time horizon:

- 1) *Reachability of patient stability*: reaching a location representing the stabilization of patient vitals;
- 2) *Duration in non-breathing state*: TV (tidal volume) remains below a defined threshold for a specified duration;
- 3) *Persistence of critical health condition*: remaining in a state with multiple vitals outside their safe ranges for a sustained period.

These properties are expressed in Metric Interval Temporal Logic (MITL) [20] formulae. The probability that the first formula holds is expected to fall below a stakeholder-defined threshold, whereas the probabilities for the second and third are evaluated to exceed their respective thresholds. Traces

reaching the sink location are not considered violations, as this represents unmodeled behaviors and an unknown system state. Alternative interpretations (e.g., treating these behaviors as failures) are possible and can be implemented by adjusting the MITL properties. We define goal G as the singleton set containing the location of the patient model representing a stable condition and the time spent in that location as the cost metric, which we aim to maximize.

2) *Model Space Analysis*: Automated techniques are adopted to systematically explore the PDP model space and identify diverse critical scenarios. Model space analysis follows an iterative process alternating between Space Exploration and Verification. As introduced above, the PDP model M is parameterized by vector φ , representing the degrees of freedom in the behavior of both the physician and device models. The exploration step is realized either by selecting an assignment to parameters φ or by changing structural features of M , yielding a modified model M' , while the verification step evaluates the probability that $M'[\varphi]$ satisfies the defined dependability requirements Ψ . These probabilities are fed back into the exploration step in a feedback loop. Specifically, the probability that models satisfy Ψ is computed through Statistical Model Checking (SMC) [36]. If the computed probability of any undesirable behavior exceeds a stakeholder-defined threshold, the model is considered a *failure*. During model space exploration, failure-inducing PDPs models (or more precisely, their parameterizations φ) are collected in a set Φ to identify critical behaviors of the physician-device system that may compromise patient safety. These failures highlight specific combinations of clinical decisions and system responses that merit further investigation, either as indicators of potential safety risks or opportunities for system improvement.

M-GENGAR supports two complementary exploration strategies: mutational *fuzzing* and *search-based* optimization (see Section II). Both strategies modify model parameters or structural elements of the SHA model and are guided by the likelihood of a model violating requirements as determined during Verification. *Mutational fuzzing* applies domain-specific mutation operators to introduce behavioral variations into the SHA, iteratively generating new *mutants*. These operators maintain model validity while producing meaningful variability. An archive of physician-device SHA mutants is maintained and enriched with new mutants added according to application-specific criteria, serving as a pool of promising candidates for further mutation. By prioritizing high-risk mutants, the algorithm directs exploration toward underexplored regions of the model space, increasing the likelihood of uncovering critical behaviors. The *search-based* strategy treats model space exploration as a multi-objective optimization problem, with each objective minimizing the probability of satisfying a specific dependability property. Unlike fuzzing, the definition of the candidates to evaluate is not generally driven by application-dependent criteria, but rather depends on the employed algorithm, which introduces variability in an application-agnostic manner (still by acting on model parameters and on the structural elements of the automata). These strategies produce a collection of physician-device variants, each representing a

distinct instantiation of model M , which are then analyzed via verification and potentially labeled as failures.

Example IV.7. In our running example, we define two mutation operators for fuzzing. The first perturbs a randomly selected parameter in φ by applying a bounded scaling factor, thereby modifying the intensivist’s reaction times or probabilistic preferences when selecting interventions in the SHA shown in Fig. 3. The second removes a randomly chosen transition, modeling situations in which the physician does not respond to a specific clinical event. We set the criterion for adding a mutant to the archive as exceeding the current maximum observed likelihood of violation for at least one requirement. An example of an alternative physician–device model removes the topmost transition (labeled by on) that activates the ventilator in response to a low oxygen saturation event, while two others increase the physician’s reaction time (e.g., $\lambda = 1/15$ and $\lambda = 2/25$), representing delayed responses due to workload or organizational factors. SMC results indicate a violation of at least one requirement (see Example IV.6), leading the corresponding models to be classified as failure-inducing scenarios. We employ the Non-dominated Sorting Genetic Algorithm II (NSGA-II) [22] as the multi-objective searching algorithm. Unlike fuzzing, candidate generation is not driven by application-dependent criteria, but is performed in a black-box manner by the algorithm, which perturbs model parameters and structure.

3) *Validation*: PDP mutants in Φ that yield a failure but represent unrealistic or clinically irrelevant scenarios are filtered out, obtaining a reduced subset of parameters $\Phi' \subseteq \Phi$. While some of these cases may technically pose risks to patient safety, they are considered either uninteresting for further analysis or unlikely to occur in real-world settings, based on stakeholder judgment. For example, a case where a physician takes an excessively long time (e.g., minutes) to respond to an emergency may be deemed unrealistic, given the high availability of personnel in typical ICU environments. Other scenarios may involve implausible clinical actions that no trained physician would reasonably perform. Because such scenarios cannot always be excluded a priori, they must be explicitly reviewed by clinical experts to assess their validity.

Example IV.8. After a guided review of the SHA components in Fig. 3, the expert identifies edges essential for any clinically reasonable procedure. Based on this review, a set of structural and parametric constraints is derived to serve as exclusion criteria. These constraints enable automated filtering of scenarios unlikely to occur in real ICU settings. For example, among the three SHA models in Example IV.7, the first is excluded as it lacks an appropriate physician response to the OS^{low} event, a behavior deemed extremely unlikely by the domain expert.

4) *Diversity Analysis*: The set of realistic failure-inducing PDP models in Φ' is subjected to a diversity analysis to identify distinct underlying root causes. Indeed, in some cases, failure-inducing models that differ syntactically may nevertheless exhibit semantic similarity, and hence fail to correspond to distinct scenarios. To reduce redundant information and obtain a reduced set of representative critical scenarios, unsupervised

clustering [52] is applied to group similar failure-inducing PDP models based on their behavioral characteristics and, from each cluster, a representative model is extracted. All the representatives collectively form the final set of diverse failure scenarios presented to stakeholders. This process requires a definition of *similarity* between models and a *selection criterion* for choosing a representative from each cluster. Both definitions are collaboratively established with domain experts to balance clinical and analytical relevance. Failure-inducing PDP models can be clustered by analyzing the parameter space defined by their associated vectors φ .

Example IV.9. We apply unsupervised hierarchical clustering using the Unweighted Pair-Group Method with Arithmetic mean (UPGMA) [52], which iteratively merges clusters based on the average pairwise distance between all elements across candidate clusters, thereby capturing similarity relationships in the parameter space. Rather than producing a single partition, UPGMA yields a dendrogram that represents the hierarchical organization of the PDP models. A concrete clustering is then obtained by cutting the dendrogram at a selected distance threshold, which allows the number and granularity of clusters to be tuned to the desired level of abstraction. In our evaluation, we consider multiple candidate clusterings with different numbers of clusters and automatically select the one that maximizes the silhouette score [50], a widely adopted metric for assessing cluster cohesion and separation.

The parameters φ of the two remaining example SHA in Example IV.8 are almost identical, differing only in the physician’s response time. Accordingly, the clustering procedure considers them to be close in the parameter space and assigns them to the same cluster. This cluster can be interpreted as the set of critical circumstances due to delayed action by the physician (i.e., slow response time). The centroid of the cluster is then selected as its representative.

C. Online Clinical Decision Support

This phase completes the implementation of the DT of the PDP triad by establishing a feedback loop between its physical and the digital copies. Specifically, the DT requires *alignment* between the physical state of the system and its digital representation through a continuous, bidirectional flow of data and corresponding state updates.

A selected model, representing the current status of the physical PDP triad in the DT loop, is translated into a Priced Timed Game Automata (PTGA), and a strategy is computed, ensuring reachability of a prescribed goal. The strategy is then used in Decision Selection, while state alignment (highlighted in blue in Fig. 2) is maintained via Digital State Identification and Physical State Actuation. The models for which the control strategy is calculated can be either the representatives produced by the diversity analysis, or generalist models that do not capture specific criticalities of the physical triad but instead represent possible nominal operating scenarios. The latter can be developed starting from the model obtained through the activity described in Section IV.1 or from its generalizations.

1) *Controller Synthesis:* Since patient safety is a primary concern, a controller is synthesized to assist the physician

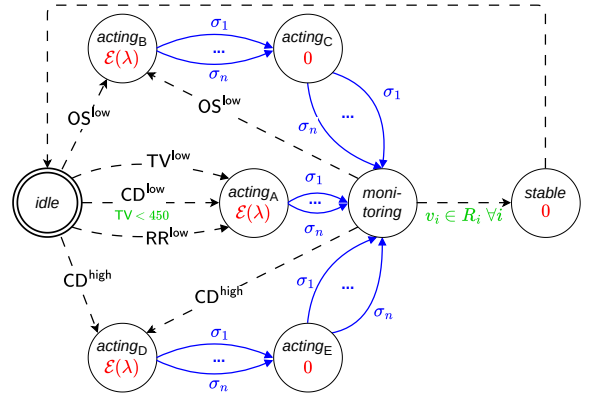


Fig. 5: Physician-device PTGA used in the running example. Solid blue edges are the physician’s controllable actions $\sigma_1, \dots, \sigma_n \in \Sigma_{o,c}$. Dashed edges are uncontrollable actions.

through recommended actions that aim at preserving patient stability. The methodology leverages game-theory techniques for which an entirely stochastic SHA model is interpreted as a 1½-player game, modeling the physician (i.e., the *player*) as a goal-oriented strategy-based player and the patient (i.e., the *adversary*) as a stochastic adversary [19]. Specifically, the SHA model is converted into a PTGA where the physician’s actions, instead of being probabilistic as in the SHA, are governed by a strategy while the patient’s reactions are stochastic. Hence, the SHA-to-PTGA conversion leaves the patient model unvaried and marks all physician’s edges as controllable.

Based on a formal PTGA representation of the system, derived from a selected model $M[\bar{\varphi}]$, the Controller Synthesis activity computes a strategy $\Pi_{M[\bar{\varphi}]}$ that prescribes the optimal action at each possible system state to satisfy the reachability goal G specified by stakeholders. The strategy serves as a physician decision-support engine in the DT alignment loop.

Example IV.10. Consider a modified version of the physician-device SHA of Fig. 3 with localized changes in each *acting* and *monitoring* location, represented in Fig. 5. This model is a generalization of the physician model shown in Fig. 3 that does not encode any specific medical procedures, yet it represents a generalized physician with full freedom to adjust the ventilator parameters. Specifically, it includes outgoing edges for all the physician-controlled actions $\sigma_1, \dots, \sigma_n$ in $\Sigma_{o,c}$, where $\Sigma_{o,c} := \{(P_j)^{up}, (P_j)^{down}\}_{P_j \in P} \cup \{on, off\}$. By definition, the PTGA configuration tuple (l, ν) includes: *i*) the current locations of both automata; *ii*) a collection of boolean variables r_i , with $\forall_i \in V$, indicating whether each patient’s vital currently falls within (T) or outside (F) its safe range R_i ; *iii*) a boolean variable r_{on} indicating whether mechanical ventilation is currently active (T) or inactive (F). The learned controller $\Pi_{M[\bar{\varphi}]}$ maximizes permanence time in the location defining goal G (see Example IV.6). One illustrative tuple-action mapping of the learned strategy is:

$$\Pi_{M[\bar{\varphi}]}(acting_A, q_9; T, T, T, T, F, F) = on.$$

The mapping states that if the physician-device SHA is currently in location *acting_A*, the patient SHA is in location

q_9 , the first four patient vitals are stable while the fifth one (TV) is not, and mechanical ventilation is inactive, the action suggested by the strategy is on, i.e., activate the ventilator.

2) *Digital State Identification*: Within the DT paradigm, a digital representation of the current state of the physical PDP triad, captured in the SHA model $M[\bar{\varphi}]$ via locations and configuration variables, is essential for enabling control feedback through recommendations and formal analysis. State identification can be achieved by: *i*) acquiring the patient's vital signals in real time, including X_M ; *ii*) applying labeling function \mathcal{L}_{X_M} , which produces a trace τ representing the events recorded in the physical environment; and *iii*) interpreting τ on the PDP model. The location reached in the SHA by sequentially firing the events from τ , and the sampled vitals, represent the digital counterpart of the current state of the physical system. The initial location of the model at the onset of the feedback loop is the one marked as *initial* in the SHA.

Example IV.11. Consider the representation of the PDP triad shown in Fig. 4 (partially) for the patient and Fig. 5 for the physician. Let us assume that, at a certain time instant, the patient's current location is q_8 and the physician's current location is *idle*, and that readings from the patient's tidal volume indicate that the metric has dropped below the critical threshold TV^{\max} . The labeling function indicates that event $\mathcal{L}_{X_M}(t_k) = TV^{\text{low}}$ has taken place. The patient and physician SHA transition to locations q_9 and *acting_A*, respectively.

3) *Decision Selection*: The actions implementing the control feedback loop are identified by means of a *decision engine*, which is based on the controller $\Pi_{M[\bar{\varphi}]}$ synthesized during the previous phase. Given the current system state (l, ν) , the engine selects an SHA event $\sigma = \Pi_{M[\bar{\varphi}]}(l, \nu) \in \Sigma_{o,c}$. This event is the formal representation of a physician's action and corresponds to the behavior that results in minimal cost when reaching goal G . The selected action is sent to the physical state actuator either as a recommendation presented to the physician through a digital interface or as a direct control signal to an automated device. Concurrently, event σ is fired in the SHA network, potentially triggering a location update in the patient and/or physician automata.

Example IV.12. The synthesized strategy prescribes the activation of the ventilator, corresponding to the firing of event $\sigma = \text{on}$. As a consequence, the physician SHA transitions from location *acting_A* to *monitoring*, and a corresponding update occurs in the patient SHA if the current state q_9 admits an outgoing transition labeled with event on.

4) *Physical State Actuation*: The actuation of the decision engine's output in the physical world can take two forms. It can be fully automated, with the actions sent directly to the device, which updates its settings accordingly and in real time. Alternatively, they can be provided as a recommendation to the physician, leaving the final decision to the physician's judgment and expertise. In either case, the decision affects the patient's physiological state and metrics, a process corresponding to the second half of the DT alignment loop.

Physical state actuation closes the DT alignment loop, as it

enables decisions produced in the digital domain to influence the physical system. It takes place entirely in the real world and depends on deployment-specific considerations, such as device interoperability, clinical workflows, and regulatory constraints. For this reason, the concrete implementation of actuation, whether fully automated or mediated by the physician, is beyond the scope of this work, which focuses on the methodological foundations for constructing and analyzing DTs. Accordingly, in Fig. 2 this activity is depicted as an external block positioned outside the third phase of the methodology.

V. EMPIRICAL EVALUATION

This section presents the experimental campaign⁴ designed to assess both the accuracy and the scalability of the proposed methodology. The evaluation is structured around the following research questions:

- RQ1:** What is the accuracy of the patient model resulting from the learning phase of M-GENGAR?
- RQ2:** What is the effectiveness of M-GENGAR in detecting realistic and diverse failure scenarios?
- RQ3:** What is the cost of the failure detection phase of M-GENGAR?
- RQ4:** What is the effectiveness of the strategies synthesized by M-GENGAR in stabilizing patient metrics?

A. Design of the evaluation

1) *Evaluation subjects*: Synthetic patient data are generated using Kitware PULSE [13], an open-source high-fidelity physiological simulator capable of reproducing diverse clinical conditions and adverse events. The simulations are executed through BREATHE [16], a framework built on PULSE that provides a clinician-oriented interface for real-time monitoring of vital signs and interactive control of ventilator settings.

Data collection to train the predictive models was carried out with the support of a physician with four years of experience in intensive care medicine. The clinician conducted 8 simulated clinical scenarios using BREATHE, for a cumulative simulation duration of 45 minutes. The executed scenarios covered 10 distinct health complications, together with the corresponding ICU interventions and resulting patient responses. During the simulations, the intensivist was provided with real-time physiological data and adjusted ventilation parameters according to their clinical judgment and established medical guidelines.

The physician also contributed to the definition of our main study subject, that is, the respiratory intensive care example introduced in Section III and Section IV, by identifying relevant physiological signals, describing medical procedures with SHA, and specifying validation criteria to discriminate clinically realistic scenarios from unrealistic ones.

2) *Methods under comparison*: We assess the cost-effectiveness of M-GENGAR by comparing it against multiple baseline methods, selected according to the specific RQ.

To evaluate the accuracy of the learned patient model (RQ1), we compare it with three mainstream regression baselines. All models share the same input-output specification: the input

⁴Replication package found at <https://doi.org/10.5281/zenodo.18430307>.

encodes a simulation trace as a sequence of events (set Σ as per IV-A), represented as categorical variables, together with the corresponding TV values associated with each event. The output is a single scalar representing the predicted TV after the last event in the trace.

The considered baseline models are: *dual-input* Neural Network (NN) [27], *XGBoost* [15], and *Elastic Net* [56]. The *dual-input* NN uses one branch to encode the categorical event sequence through an embedding layer followed by an LSTM layer [32], while the second branch processes the TV values using a convolutional layer followed by pooling. The outputs of the two branches are concatenated and passed through a fully connected layer with dropout to mitigate overfitting. The *XGBoost* is a gradient-boosted decision tree model operating on a combined input vector that includes both the encoded event sequence and the corresponding TV values. The *Elastic Net* is a linear regression model with combined L^1 and L^2 regularization (same input representation as XGBoost).

We evaluate the effectiveness (RQ2) as well as the cost (RQ3) of M-GENGAR in detecting realistic and diverse failure scenarios by comparing alternative strategies for exploring the PDP model space. Specifically, we compare the proposed approaches—*mutational fuzzing* and a *search-based* strategy based on NSGA-II—against a *random search* baseline, which uniformly samples random mutations over both model parameters and structural elements.

Concerning the effectiveness of the strategies to stabilize the patients (RQ4), we compare M-GENGAR against a ground-truth decision-making process of a real human physician.

3) *Statistical tests*: We reduce the risk of obtaining results by chance evaluating 20 distinct scenarios and executing each exploration strategy 20 times under the same budget constraints (i.e., producing a total of 500 patient model mutants). Preliminary tests indicate that this budget is adequate to reach a performance plateau during model space exploration. Following the guideline by Arcuri and Briand [4], we employ the non-parametric Mann–Whitney U test [40] to assess the statistical significance of our results. Additionally, we calculate Vargha and Delaney’s \hat{A}_{12} score [54] to measure the effect size between two samples, offering an indication of stochastic dominance. We categorize the effect size \hat{A}_{12} ($= 1 - \hat{A}_{21}$) using the following standard classes: small (S), medium (M), or large (L) when its value is at least 0.56, 0.64, or 0.71, respectively; none (N) otherwise.

4) *Evaluation testbed*: All experiments were executed on an Ubuntu 24.10 system with standard hardware: an 8-core Intel Core i5 processor at 4.2GHz and 16 GB of RAM.

B. Evaluation results

1) *Model accuracy (RQ1)*: We assess the accuracy of the model learned with L_{SHA}^* by observing the variable governed by flow conditions, specifically $TV \in X_F$, in the patient SHA. The test set consists of 20 scenarios encompassing health complications of different types and severities, along with a sequence of events describing the onset of a particular health complication and randomly chosen physician actions. Each scenario is simulated in BREATHE to obtain the actual

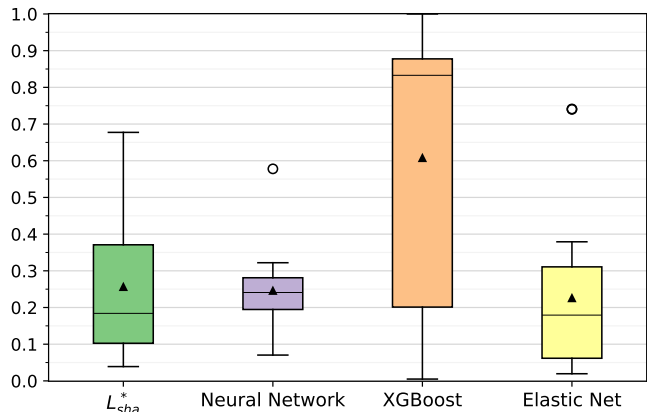


Fig. 6: RQ1 MAPE values for each regression model.

TABLE II: Results of statistical tests for regression (RQ1).

	p -val	\hat{A}_{12}
L_{SHA}^* vs Neural Network	3.97e-01	S
L_{SHA}^* vs XGBoost	9.35e-03	L
L_{SHA}^* vs Elastic Net	4.83e-01	S
Neural Network vs XGBoost	2.27e-02	L
Neural Network vs Elastic Net	2.09e-01	S
XGBoost vs Elastic Net	5.54e-03	L

final TV values as ground truth that we used to compare the predicted TV value obtained from the learned patient SHA, coupled with the complete physician-device SHA from Fig. 3, and the trained baseline regressors. The SHA modeling PDP triads are translated into UPPAAL models [6], from which we extract the predicted TV at the end of each trace.

We evaluate our PDP model against the baselines on two prediction tasks: *regression* and *classification*. For the *regression* task, we calculate each model’s test-set Mean Absolute Percentage Error (MAPE) relative to the ground truth.

Results. Figure 6 shows the distribution of MAPE for each model, while Table II provides the Mann–Whitney p -values and Vargha–Delaney effect sizes (\hat{A}_{12}). For *classification*, we discretize the regression outputs into three categories (*low*, *ok*, *high*) based on their position relative to TV’s safe operating range, as defined in Example IV.1. Classification accuracy is then computed as the proportion of correctly classified samples. Table III collects relevant metrics for both prediction tasks, namely median MAPE, mean MAPE, and classification accuracy.

The L_{SHA}^* model consistently outperforms XGBoost in both regression and classification tasks. Its average MAPE is similar

TABLE III: Scores for regression and classification (RQ1).

model	regression (MAPE)		classification
	median	mean	accuracy
L_{SHA}^*	0.184	0.258	0.90
Neural Network	0.241	0.247	0.40
XGBoost	0.833	0.609	0.30
Elastic Net	0.179	0.227	0.70

to that of the NN and Elastic Net models, though statistical testing does not allow us to reject the null hypothesis that these three models share the same MAPE distribution. We can observe that L_{SHA}^* achieves substantially higher classification accuracy, more than twice that of the NN, suggesting a deeper understanding of the underlying phenomenon.

RQ1 summary. The SHA learned by L_{SHA}^* outperforms all three baseline models: dual-input Neural Network (NN), XGBoost, and Elastic Net. This advantage is especially clear in classification, where L_{SHA}^* reaches accuracy levels up to $3\times$ higher. For regression, L_{SHA}^* performs on par with the NN and Elastic Net, while reducing average error by $3\text{--}4\times$ relative to XGBoost.

2) *Effectiveness of failure detection (RQ2):* We measure effectiveness by counting the occurrences of *different* failure-inducing scenarios discovered during PDP space exploration, along with evaluating their realism. Using the complete physician–device model shown in Fig. 3, we apply the mutation operators outlined in Section IV: parameter perturbation with a mutation factor of $k = 1.5$ (while respecting parameter bounds) and edge removal. All methods are executed under the same computational budget of 500 generated mutants (corresponding to 50 generations of 10 individuals each for the search-based strategy). For each technique and requirement, we filter out failure cases that are not clinically realistic according to the criteria defined by the domain expert, as described in Section IV (see Example IV.8). We then compute the rate of realistic failure cases over the total budget.

To assess the diversity of the identified failures, we apply the clustering procedure (see Example IV.9) to the set of realistic failure cases. We evaluate clusterings composed of up to 20 clusters and select the one that maximizes the silhouette score. The resulting number of clusters is used as a surrogate measure of failure diversity, capturing the extent to which a technique explores distinct regions of the model space and uncovers qualitatively different classes of clinically relevant failures. For both failure detection rate and number of clusters, higher values indicate better performance, as they reflect a greater ability to uncover a wide variety of critical scenarios.

Results. Figure 7 shows the distributions of the number of realistic failures identified by each technique over 20 repetitions. Similarly, Fig. 8 reports the distributions of cluster cardinalities across repetitions. Table IV presents statistical significance and effect size for all pairwise comparisons, considering both the number of realistic failures and the number of clusters.

Mutational fuzzing identifies proportions of realistic failure scenarios ranging between 15 and 65% across different requirements. In particular, fuzzing detects failures in approximately 60% of cases (median value) for Requirement 1 and 35% for Requirements 2 and 3. It also achieves the largest number of distinct clusters, with median values (18–19) close to the maximum number of clusters evaluated across all requirements. Statistical tests confirm this superiority in all cases except one, i.e., the comparison against random search for the number of clusters derived from Requirement 1.

The failure detection rate of the search-based approach is

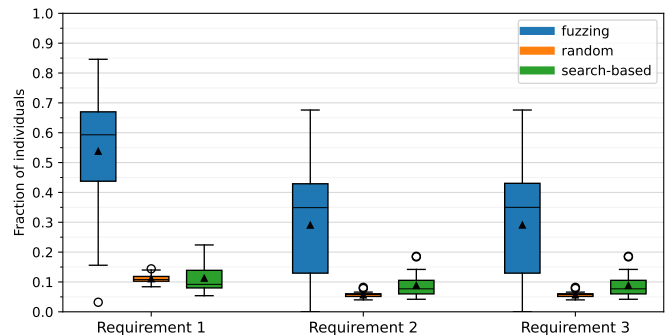


Fig. 7: Detection rate of realistic failures for each requirement and exploration technique (RQ2).

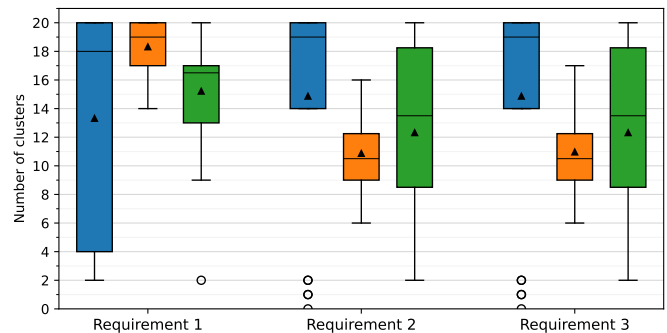


Fig. 8: Number of clusters for each requirement and exploration technique (RQ2). Color code is the same as Fig. 7.

much lower than fuzzing, around 10% for all requirements. This trend also holds for the number of clusters, sometimes comparable but lower on average. In this sense, performance of the search-based approach is comparable to random search.

Overall, the results suggest that fuzzing is the most effective technique for uncovering a larger number of realistic and distinct failure scenarios. Better performance of fuzzing compared to the search-based approach can be explained by the formulation of the optimization objective, i.e., the minimization of requirement satisfaction probability. This objective tends to drive the search-based approach toward simpler models (e.g., with fewer transitions), concentrating exploration near global optima in the parameter space. Such

TABLE IV: Statistical tests for model space exploration and clustering (RQ2).

Realistic failures	Requirement 1		Requirement 2		Requirement 3	
	p -val	\hat{A}_{12}	p -val	\hat{A}_{12}	p -val	\hat{A}_{12}
fuzzing vs random	1.19e-06	L	1.22e-03	L	1.22e-03	L
fuzzing vs search-based	2.35e-06	L	3.04e-03	L	3.04e-03	L
random vs search-based	1.98e-01	S	5.87e-03	L	6.86e-03	L
Clustering	Requirement 1		Requirement 2		Requirement 3	
	p -val	\hat{A}_{12}	p -val	\hat{A}_{12}	p -val	\hat{A}_{12}
fuzzing vs random	3.85e-01	S	6.71e-03	L	6.71e-03	L
fuzzing vs search-based	6.49e-01	N	8.29e-02	M	8.29e-02	M
random vs search-based	2.87e-03	L	1.54e-01	S	1.62e-01	S

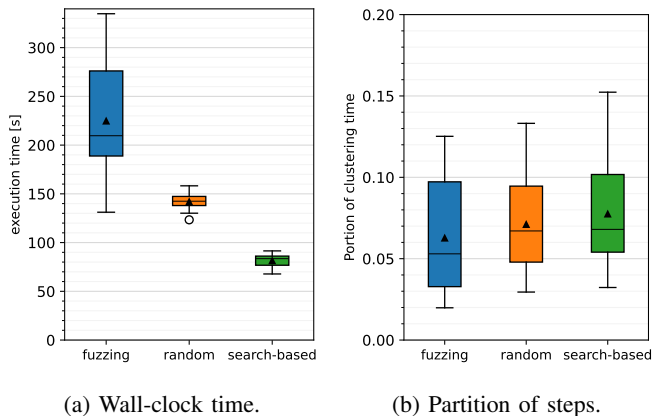


Fig. 9: Cost of exploration techniques in execution time (RQ3).

models are likely to violate the specified requirements, yet they typically lead to clinically unrealistic behaviors. This plausibly explains the substantial discrepancy between the total number of detected failures and those deemed clinically realistic.

RQ2 summary. Fuzzing consistently outperforms both the search-based approach and random search, identifying the highest proportion of realistic failure scenarios (median values between 35-60% across requirements) and producing more clusters (median values 18 – 19). The other methods yield substantially fewer realistic failures (around 10%) and less clusters (median values between 10-16).

3) *Cost of failure detection (RQ3):* We use the same setup as in RQ2, but evaluate cost in terms of wall-clock execution time. We record the execution time of both model space analysis and clustering for each method under comparison.

Results. Figure 9a shows the distribution of execution time across 20 repetitions. The cost of fuzzing is generally higher and exhibits a higher variance (ranging from 2 to 6 minutes) compared to the other methods. The search-based approach is the most time-efficient, typically finishing just over 1.5 minutes, while random search averages around 2.5 minutes. Such efficiency can be attributed to its optimization objective, which explicitly minimizes requirement satisfaction probability. As anticipated above (see RQ2), this objective steers the search toward simpler yet unrealistic models. Such models are likely to violate the requirements and are usually faster to evaluate.

Overall, most of the execution time is spent performing SMC with UPPAAL, while the time overhead for mutant generation is generally negligible. The clustering activity also represents a small fraction of the total time, usually around 5-10%, as shown in Fig. 9b.

RQ3 summary. The search-based approach is the most time-efficient method, completing significantly faster than both fuzzing and random search, largely due to its optimization toward simpler models that are quicker to evaluate. Execution time is dominated by SMC, with mutant generation and clustering contributing only marginal overhead.

TABLE V: Deviation compared to nominal TV = 400 ml (RQ4). The bottom row shows average values.

Human physician		Controller	
absolute Δ [ml]	relative Δ [%]	absolute Δ [ml]	relative Δ [%]
201	50.2	39	9.7
282	70.5	39	9.7
237	59.2	224	56.0
197	49.2	197	49.2
400	100.0	400	100.0
216	54.0	39	9.7
400	100.0	400	100.0
124	31.0	36	9.0
257.1	64.2	171.7	42.9

4) *Effectiveness of stabilization strategies (RQ4):* We assess the effectiveness of the proposed stabilization strategies by analyzing the patient’s physiological state after the application of each strategy and comparing it against the outcome achieved by a human physician under the same clinical conditions.

To apply the strategies, we synthesized an automated controller using UPPAAL STRATEGO [18]. To ensure statistical robustness, we repeat the strategy synthesis process 20 times, verifying that the resulting strategies lead to consistent and reproducible outcomes. We then execute 8 simulated clinical scenarios in BREATHE, reproducing the health complications previously presented to the physician. In each scenario, BREATHE’s mechanical ventilator is automatically controlled according to the synthesized strategy, with patient states periodically matched against the mapping table to trigger the corresponding control actions.

At the end of a fixed observation period, we analyze the patient’s physiological state by counting the number of monitored patient vital signals $v_i \in V$ that lie within their predefined safe operating ranges R_i , and comparing this count against the human baseline. We consider a strategy as *successful* if it stabilizes at least as many vital signals as the human physician. In addition, we analyze the behavior of TV, the variable governed by flow conditions in the SHA models. For each scenario, we record the TV value from BREATHE at the end of the observation period under the synthesized strategy and compare it against the simulated patient’s nominal healthy value (equal to 400 ml for all scenarios); the physician’s outcomes are evaluated using the same criterion.

Results. Overall, the application of the strategies synthesised by M-GENGAR is successful in 7 out of 8 scenarios. Table V reports the deviation Δ of the observed TV values from the nominal reference, expressed as both relative and absolute errors across all 8 scenarios, with average values summarized in the final row. On average, the automated controller maintains TV approximately 20% closer to the corresponding nominal value compared to the human physician.

RQ4 summary. The stabilization strategies synthesized by M-GENGAR are successful in most cases, matching or outperforming the human physician. On average, the automated controller maintains TV approximately 20% closer to its nominal healthy value, indicating comparable, and often improved, physiological stabilization relative to human-driven interventions.

VI. DISCUSSION

A. Threats to Validity

Threats to external validity arise from the use of a single evaluation subject. We mitigate this threat by considering a wide variety of simulated clinical scenarios covering multiple health complications with varying severity levels, all validated by a physician with four years of working experience in intensive care units. All experiments rely on synthetic data generated by the PULSE physiological engine, which is a high-fidelity simulator widely used for medical training and research. The learning and validation phases involve a single physician, which may limit the generalizability of clinical judgments and realism criteria used to detect plausible failures.

To mitigate internal validity threats, all techniques are evaluated under identical computational budgets, identical mutation operators, and identical sets of requirements. Each stochastic method is executed multiple times, and statistical testing is applied to reduce the risk of obtaining results by chance [4].

As reported in Section V, the search-based approach is optimized toward minimizing requirement satisfaction probability, which may bias it toward simpler and faster-to-evaluate models. While this behavior is intrinsic to the optimization objective and intentionally analyzed, it may partially explain performance differences and must be considered when interpreting effectiveness and cost results. Similarly, clustering-based diversity assessment depends on the chosen distance metric and clustering parameters, which may influence absolute cluster counts, although relative comparisons remain consistent across techniques.

Concerning the effectiveness of the strategies synthesized by M-GENGAR, we measured the number of stabilized vital signs and the deviation of TV from its nominal healthy value. This metric captures short-term physiological stabilization but does not account for possible longer-term outcomes (or secondary clinical objectives). As a consequence, reported results should be interpreted as indicators of stabilization capability rather than comprehensive clinical optimality. Furthermore, we assume that the actions selected by the synthesized controller are always applied to the patient. This assumption models a deployment scenario in which the physician fully accepts the recommendations of a clinical decision support system, deliberately excluding cases of partial compliance or override. Under this assumption, the reported results can be interpreted as a lower bound stabilization capability. Real-world effectiveness will depend on human-DT interaction dynamics, which are outside the scope of this study.

We mitigate conclusion validity threats by repeating experiments across multiple runs and scenarios, applying non-

parametric statistical tests where applicable, and reporting effect sizes alongside statistical significance.

B. Impact

This work contributes to the SAFEST project⁵ by advancing trustworthy DT-based methodologies for medical CPSs under uncertainty and heterogeneity. By integrating probabilistic modeling, automated exploration of critical contingencies, and strategy synthesis within a closed-loop DT architecture, the methodology increases confidence in DT-driven decision support despite incomplete data and modeling approximations. The explicit treatment of uncertainty and the modular representation of actors support sound dependability analysis while managing the complexity of heterogeneous DT components.

The work also highlights two complementary needs central to SAFEST. First, effective DT-based analyses rely on reliable physiology simulators [12], [16] to generate realistic data and stress-test rare critical conditions. Second, automating the extraction of medical procedures and guidelines into machine-readable representations reduces ambiguity in practitioner behavior. Approaches such as MARACTUS [30] address this need by transforming unstructured clinical documents into analyzable action models for integration into model-driven pipelines and CDSSs. Together, these directions strengthen the SAFEST vision of dependable DT-based healthcare solutions.

VII. RELATED WORK

A review of the existing literature reveals that no prior study directly mirrors the approach proposed in this paper. A DT-oriented architectural solution to formalizing the PDP triad is introduced by Bersani et al. [7], [8]. Their approach emphasizes trust, defined as alignment between physical systems and DTs, and includes mechanisms for validating performance under human and environmental uncertainty [7], a high-level reference architecture, and reliability estimation tools [8]. Nonetheless, their work remains conceptual and lacks empirical evaluation.

The DT concept originally introduced by Grieves [28] has matured substantially, especially in manufacturing contexts. Abanda et al. [1] survey ten DT definitions from 2012 to 2022, illustrating this evolution. With increasing human involvement in industrial processes, DTs began to model human aspects, leading to the development of Human Digital Twins (HDTs). Gaffinet et al. [26] review ten surveys on HDTs, highlighting their expansion across domains. Miller et al. [43] define HDT as a digital representation of a human combining mechanistic and statistical models, covering cognition, personality, and behavior. Latif et al. [34] provide a domain-specific example of human-performed process modeling. Lin et al. [39] survey HDT technologies and propose a general architecture, focusing on modeling human activity and social behavior, but omitting task-based workflows such as medical procedures, which our model explicitly incorporates.

Asad et al. [5] examine Human-Centric DTs, noting that while ergonomics and health are addressed, cognitive processes and decision-making are generally overlooked. Wang

⁵<https://safest-prin.github.io>

et al. [55] similarly highlight the overemphasis on physical assets at the expense of human modeling, proposing a layered HDT architecture within which our SHA-based patient model fits. Our approach, however, introduces SMC-based analysis, adding capabilities absent from their taxonomy. Li et al. [31] present a DT-based framework for ergonomic analysis, focusing on body movement and cognition. Their “Digital Engine” includes simulation and analysis components, mapping closely to our SHA-based models and SMC-driven dependability evaluation. Lauer-Schmaltz et al. [35] review HDTs for behavioral therapy and rehabilitation, noting limited treatment of motivational and cognitive mechanisms. Our work goes further by explicitly capturing medical knowledge and procedural workflows. Sahal et al. [51] propose a Personal DT integrating blockchain and AI to support decision-making, though at a high level. They identify healthcare requirements such as clinical decision support and analysis. Our system can be seen as a concrete realization of these goals.

Katsoulakis et al. [33] survey healthcare-focused DTs, primarily addressing patient care and organ-specific modeling for personalized medicine. One application area, namely hospital management and care coordination, includes hospital workflows and staff modeling, aligning with our approach. Yet, none of the surveyed works incorporate automata-based models or testing-inspired analysis, highlighting our contribution. Chen et al. [14] review communication technologies for HDTs in personalized healthcare, providing low-level networking insights not covered here. Likewise, Papachristou et al. [47] review DTs for precision medicine, covering diagnosis, surgery, and therapy, but do not address task-oriented physician modeling as we do.

Roopa and Venugopal [49] focus on DTs in Cyber-Physical Healthcare Systems (DT-CPHS), identifying operational efficiency as a key requirement. Our system contributes by detecting critical scenarios in intensive care caused by physician misbehavior, enhancing care delivery. Croatti et al. [17] integrate DTs with Multi-Agent Systems for smart healthcare, modeling heterogeneous entities and supporting trauma care, but their DT primarily aids documentation and procedure tracking without advanced analytics. Mariani et al. [42] extend this work conceptually, discussing simulation and prediction, yet without concrete implementation. While aligned with representing the PDP triad through DTs, our approach delivers a more operational and grounded realization.

Mohamed et al. [44] propose a DT framework for healthcare systems engineering, including patients, staff, and facilities, but model physicians and processes more as administrative units than as knowledge-driven clinical agents. Our approach captures both behavioral dynamics and medical expertise of physicians within the DT. Elayan et al. [24] and Rahim et al. [48] both implement ECG classifiers in DT frameworks. Elayan et al. focus on real-time machine learning for heart disease diagnosis using IoT-integrated DTs, with healthcare improvements treated as secondary. Rahim et al. present a Smart Medical CPS for hospitals, integrating patients, devices, and staff. Their system supports arrhythmia diagnosis via ECG classification and provides monitoring tools for healthcare professionals. While both works offer predictive functionality,

our approach uniquely integrates formal task modeling and automated analysis to identify critical care scenarios.

VIII. CONCLUSION

M-GENGAR is an extended reliability-engineering methodology for the dependability analysis and attainment of critical PDP systems in healthcare, operating within a closed-loop DT paradigm. By combining data-driven learning of patient dynamics with automata-based modeling, statistical model checking, model-space exploration, and diversity analysis, M-GENGAR can systematically identify, classify, and mitigate clinically plausible failure scenarios. Fuzzing-based model-space exploration outperforms baseline approaches, detecting 35–60% realistic failure scenarios and producing richer clusters of critical contingencies (median 18–19 versus 10–16). Synthesized strategies stabilize patient vitals at least as effectively as human decision-making in 87.5% of evaluated cases, keeping relevant metrics closer to nominal healthy values.

Scaling M-GENGAR to more complex clinical settings and enriching human-in-the-loop models with cognitive and team-level factors are future works. Additional directions include improving robustness under partial observability, tighter integration with high-fidelity physiology simulators, and further automation of clinical procedure extraction.

ACKNOWLEDGMENTS

This work was partially supported by the PRIN project SAFEST (award No: 20224AJBLJ) funded by the Italian Ministry of Education, Universities, and Research (MIUR).

REFERENCES

- [1] F. Henry Abanda, N. Jian, Selorm Adukpo, Valerian Vanessa Tuhaie, and Marcelline Blanche Manjia. Digital twin for product versus project lifecycles’ development in manufacturing and construction industries. *J. Intell. Manuf.*, 36(2):801–831, 2025.
- [2] Rajeev Alur, Costas Courcoubetis, Nicolas Halbwachs, Thomas A Henzinger, Pei-Hsin Ho, Alfredo Nicollin, Xavier Olivero, Joseph Sifakis, and Sergio Yovine. The algorithmic analysis of hybrid systems. *TCS*, 138(1):3–34, 1995.
- [3] Dana Angluin. Learning regular sets from queries and counterexamples. *Inf. Comput.*, 75(2):87–106, 1987.
- [4] Andrea Arcuri and Lionel Briand. A practical guide for using statistical tests to assess randomized algorithms in software engineering. In *Intl. Conf. on Software Engineering*, page 1–10. ACM, 2011.
- [5] Usman Asad, Madeeha Khan, Azfar Khalid, and Waqas Akbar Lughmani. Human-centric digital twins in industry: A comprehensive review of enabling technologies and implementation strategies. *Sensors*, 2023.
- [6] Gerd Behrmann, Alexandre David, and Kim G Larsen. A tutorial on uppaal. *Formal methods for the design of real-time systems*, pages 200–236, 2004.
- [7] Marcello M. Bersani, Chiara Braghin, Vittorio Cortellessa, Angelo Gargantini, Vincenzo Grassi, F. Lo Presti, Raffaella Mirandola, Alfonso Pierantonio, Elvinia Riccobene, and Patrizia Scandurra. Towards trust-preserving continuous co-evolution of digital twins. In *Intl. Conf. on Software Architecture Companion*, pages 96–99. IEEE, 2022.
- [8] Marcello M. Bersani, Chiara Braghin, Angelo Gargantini, Raffaella Mirandola, Elvinia Riccobene, and Patrizia Scandurra. Engineering of trust analysis-driven digital twins for a medical device. In *Software Architecture. ECSA*, pages 467–482. Springer, 2022.
- [9] Andrew D Bersten and Jonathan Handy. *Oh’s Intensive Care Manual E-Book*. Elsevier Health Sciences, 2013.
- [10] Marcel Böhme, Van-Thuan Pham, Manh-Dung Nguyen, and Abhik Roychoudhury. Directed greybox fuzzing. In *Proceedings of the 2017 ACM SIGSAC Conference on Computer and Communications Security*, page 2329–2344, New York, NY, USA, 2017. ACM.

- [11] Marcel Böhme, Van-Thuan Pham, and Abhik Roychoudhury. Coverage-based greybox fuzzing as markov chain. In *ACM SIGSAC Conf. on Computer and Communications Security*, page 1032–1043. ACM, 2016.
- [12] Andrea Bombarda, Silvia Bonfanti, Angelo Gargantini, and Elvinia Riccobene. Simspire: A simulator of the respiratory system. *IEEE Access*, 2025.
- [13] Aaron Bray, Jeffrey B. Webb, Andinet Enquobahrie, Jared Vicory, Jerry Heneghan, Robert Hubal, Stephanie TerMaath, Philip Asare, and Rachel B. Clipp. Pulse Physiology Engine: an Open-Source Software Platform for Computational Modeling of Human Medical Simulation. *SN Comprehensive Clinical Medicine*, 1(5):362–377, 2019.
- [14] Jiayuan Chen, Changyan Yi, Samuel D. Okegbile, Jun Cai, and Xuemin Shen. Networking architecture and key supporting technologies for human digital twin in personalized healthcare: A comprehensive survey. *Commun. Surveys Tuts.*, 26(1):706–746, 2024.
- [15] Tianqi Chen and Carlos Guestrin. Xgboost: A scalable tree boosting system. In *KDD Proc.*, pages 785–794, 2016.
- [16] Alessandro Colombo, Gionatha Pirola, and Angelo Gargantini. BREATHE - Biomedical Respiratory Engine for Advanced Training and Human Evaluation. <https://github.com/GionathaPirola/BREATHE>, 2025.
- [17] A. Croatti, M. Gabellini, S. Montagna, and A. Ricci. On the integration of agents and digital twins in healthcare. *Journal of Medical Systems*, 44, 2020.
- [18] Alexandre David, Peter G Jensen, Kim Guldstrand Larsen, Axel Legay, Didier Lime, Mathias Grund Sørensen, and Jakob H Taankvist. On time with minimal expected cost! In *International Symposium on Automated Technology for Verification and Analysis*, pages 129–145. Springer, 2014.
- [19] Alexandre David, Peter Gjø Jensen, Kim Guldstrand Larsen, Marius Mikučionis, and Jakob Haahr Taankvist. Uppaal stratego. In *International Conference on Tools and Algorithms for the Construction and Analysis of Systems*, pages 206–211. Springer, 2015.
- [20] Alexandre David, Kim G Larsen, Axel Legay, Marius Mikučionis, Danny Bøgested Poulsen, Jonas Van Vliet, and Zheng Wang. Statistical model checking for networks of priced timed automata. In *FORMATS*, pages 80–96. Aalborg, Denmark, 2011. Springer.
- [21] Alexandre David, Kim Guldstrand Larsen, Axel Legay, Marius Mikučionis, and Danny Bøgested Poulsen. Synthesis of optimal strategies for duration probabilistic automata. In Natasha Sharygina and Helmut Veith, editors, *Computer Aided Verification - 25th International Conference, CAV 2013, Saint Petersburg, Russia, July 13-19, 2013. Proceedings*, volume 8044 of *Lecture Notes in Computer Science*, pages 273–289. Springer, 2013.
- [22] Kalyanmoy Deb, Amrit Pratap, Sameer Agarwal, and TAMT Meyarivan. A fast and elitist multiobjective genetic algorithm: Nsga-ii. *IEEE Transactions on Evolutionary Computation*, 6(2):182–197, 2002.
- [23] Dheeraj Kumar Dhaked and Valayapathy Lakshmi Narayanan. *Recent Trends in Medical Cyber-Physical System—A Brief Survey*, pages 39–54. Springer Nature Singapore, Singapore, 2024.
- [24] Haya Elayan, Moayad Aloqaily, and Mohsen Guizani. Digital twin for intelligent context-aware iot healthcare systems. *IEEE Internet of Things Journal*, PP:1–1, 2021.
- [25] Myron D Fottler, John D Blair, Carlton J Whitehead, Michael D Laus, and Grant T Savage. Assessing key stakeholders: who matters to hospitals and why? *Journal of Healthcare Management*, 1989.
- [26] Ben Gaffinet, Jana Al Haj Ali, Yannick Naudet, and Hervé Panetto. Human digital twins: A systematic literature review and concept disambiguation for industry 5.0. *Computers in Industry*, 166:104230, 2025.
- [27] Ian Goodfellow, Yoshua Bengio, Aaron Courville, and Yoshua Bengio. *Deep learning*, volume 1. MIT Press Cambridge, 2016.
- [28] Michael W. Grieves. Product lifecycle management: the new paradigm for enterprises. *Intl. Jnl. of Product Development*, 2(1/2):71–84, 2005.
- [29] Bruno Guindani, Matteo Camilli, Livia Lestingi, and Marcello Maria Bersani. Detecting Dependability Failures in Healthcare Scenarios via Digital Shadows. In *IEEE 36th International Symposium on Software Reliability Engineering (ISSRE)*, pages 502–513. IEEE, 2025.
- [30] Bruno Guindani, Matteo Camilli, Livia Lestingi, and Marcello Maria Bersani. Agentic Generation of Structured Clinical Specifications for Digital Healthcare Services. In *IEEE/ACM 48th International Conference on Software Engineering (ICSE-SEIS)*. ACM, In-press, 2026.
- [31] Qiqi He, Li Li, Dai Li, Tao Peng, Xiangying Zhang, Yincheng Cai, Xujun Zhang, and Renzhong Tang. From digital human modeling to human digital twin: Framework and perspectives in human factors. *Chinese Journal of Mechanical Engineering*, 37:1–14, 2024.
- [32] Sepp Hochreiter and Jürgen Schmidhuber. Long short-term memory. *Neural computation*, 9(8):1735–1780, 1997.
- [33] E. Katsoulakis, Q. Wang, H. Wu, L. Shahriyari, R. Fletcher, J. Liu, L. E. K. Achenie, H. Liu, P. Jackson, Y. Xiao, T. Syeda-Mahmood, R. Tuli, and J. Deng. Digital twins for health: a scoping review. *NPJ Digital Medicine*, 7, 2024.
- [34] Hasan Latif, Guodong Shao, and Binil Starly. A case study of digital twin for a manufacturing process involving human interactions. In *Winter Simulation Conference*, pages 2659–2670, 2020.
- [35] Martin Wolfgang Lauer-Schmaltz, Philip J. Cash, John Paulin Hansen, and A. M. Maier. Designing human digital twins for behaviour-changing therapy and rehabilitation: A systematic review. *Proceedings of the Design Society*, 2:1303 – 1312, 2022.
- [36] Axel Legay, Benoît Delahaye, and Saddek Bensalem. Statistical model checking: An overview. In *RV10 Proc.*, pages 122–135. Springer, 2010.
- [37] Livia Lestingi, Marcello M Bersani, and Matteo Rossi. Model-driven development of service robot applications dealing with uncertain human behavior. *IEEE Intelligent Systems*, 37(6):48–56, 2022.
- [38] Livia Lestingi, Nicla Frigerio, Marcello M Bersani, Andrea Matta, and Matteo Rossi. Data-driven energy modeling of machining centers through automata learning. *IEEE Transactions on Automation Science and Engineering*, 2024.
- [39] Yujia Lin, Liming Chen, Aftab Ali, Christopher Nugent, Ian Cleland, Rongyang Li, Jianguo Ding, and Huansheng Ning. Human digital twin: a survey. *Journal of Cloud Computing*, 13, 2024.
- [40] H. B. Mann and D. R. Whitney. On a test of whether one of two random variables is stochastically larger than the other. *The Annals of Mathematical Statistics*, 18(1):50–60, 1947.
- [41] Valentin J.M. Manès, HyungSeok Han, Choongwoo Han, Sang Kil Cha, Manuel Egele, Edward J. Schwartz, and Maverick Woo. The art, science, and engineering of fuzzing: A survey. *IEEE Transactions on Software Engineering*, 47(11):2312–2331, 2021.
- [42] Stefano Mariani, Marco Picone, and Alessandro Ricci. Agents and digital twins for the engineering of cyber-physical systems: opportunities, and challenges. *Annals of Mathematics and Artificial Intelligence*, 92:1–22, 2023.
- [43] Michael Miller and Emily Spatz. A unified view of a human digital twin. *Human-Intelligent Systems Integration*, 4:23–33, 2022.
- [44] Nader Mohamed, Jameela Al-Jaroodi, Imad Jawhar, and Nader Kesserwan. Leveraging digital twins for healthcare systems engineering. *IEEE Access*, 11:69841–69853, 2023.
- [45] Institute of Medicine (US) Committee on Quality of Health Care in America. *To Err is Human: Building a Safer Health System*. National Academies Press (US), Washington, DC, 2000.
- [46] William Owens. *The ventilator book*. First Draught Press, 2018.
- [47] Konstantinos Papachristou, Paraskevi F. Katsakiori, Panagiotis Papadimitroulas, Lidia Strigari, and George C. Kagadis. Digital twins’ advancements and applications in healthcare, towards precision medicine. *Journal of Personalized Medicine*, 14(11), 2024.
- [48] Messaoud Rahim, Wassila Lalouani, Elbahi Toubal, and Lloyd Emokpae. A digital twin-based platform for medical cyber-physical systems. *IEEE Access*, 12:174591–174607, 2024.
- [49] M. S. Roopa and K. R. Venugopal. Digital twins for cyber-physical healthcare systems: Architecture, requirements, systematic analysis, and future prospects. *IEEE Access*, 13:44963–44996, 2025.
- [50] Peter J Rousseeuw. Silhouettes: a graphical aid to the interpretation and validation of cluster analysis. *Journal of computational and applied mathematics*, 20:53–65, 1987.
- [51] Radhya Sahal, Saeed H. Alsamhi, and Kenneth N. Brown. Personal digital twin: A close look into the present and a step towards the future of personalised healthcare industry. *Sensors*, 22(15), 2022.
- [52] Robert R Sokal, Charles D Michener, et al. A statistical method for evaluating systematic relationships. *Scientific Bulletin*, 1958.
- [53] R. Sutton, D. Pincock, D. Baumgart, D. Sadowski, R. Fedorak, and K. Kroeker. An overview of clinical decision support systems: benefits, risks, and strategies for success. *npj Digital Medicine*, 3(1):17, 2020.
- [54] Andrés Vargha and Harold D. Delaney. A critique and improvement of the "cl" common language effect size statistics of mcgraw and wong. *Journal of Educational and Behavioral Statistics*, 25(2):101–132, 2000.
- [55] Baicun Wang, Huiying Zhou, Xingyu Li, Geng Yang, Pai Zheng, Ci Song, Yixiu Yuan, Thorsten Wuest, Huayong Yang, and Lihui Wang. Human digital twin in the context of industry 5.0. *Robot. Comput.-Integr. Manuf.*, 85(C), 2024.
- [56] Hui Zou and Trevor Hastie. Regularization and variable selection via the elastic net. *Journal of the Royal Statistical Society Series B: Statistical Methodology*, 67(2):301–320, 2005.